Available online at www.sciencedirect.com
ScienceDirect
International Journal of Heat and Mass Transfer 50 (2007) 2364–2375
International Journal of HEAT and MASS TRANSFER
www.elsevier.com/locate/ijhmt

Pressure drop and heat transfer of square pin-fin arrays in in-line and staggered arrangements

Tzer-Ming Jeng [a,*], Sheng-Chung Tzeng [b]

[a] Department of Mechanical Engineering, Air Force Institute of Technology, GangShan 820, Taiwan, ROC
[b] Department of Mechanical Engineering, Chienkuo Technology University, ChanGhua 500, Taiwan, ROC

Received 31 March 2006; received in revised form 21 October 2006
Available online 21 December 2006

Abstract

This work experimentally studied the pressure drop and heat transfer of a square pin-fin array in a rectangular channel by using the transient single-blow technique. The variable parameters are the relative longitudinal pitch ($X_L = 1.5, 2, 2.8$), the relative transverse pitch ($X_T = 1.5, 2, 2.8$) and the arrangement (in-line or staggered). Compared with the open articles, the present relative pitches are smaller and independently variable. The performance of the square pin-fins as the cooling devices is compared with that of the circular pin-fins. Besides, empirical formulas for the pressure loss and the heat transfer are suggested. Finally, the optimal inter-fin pitches are provided based on the largest Nusselt number under the same pumping power, while the optimal inter-fin pitches of square pin-fins are $X_T = 2$ and $X_L = 1.5$ for the arrays in in-line arrangements as well as $X_T = 1.5$ and $X_L = 1.5$ for the arrays in staggered arrangements.

Keywords: Pressure drop; Heat transfer; Square pin-fin array; Optimal inter-fin pitch

1. Introduction

Installing pin-fins on a heating surface can increase the surface area of dissipation and cause turbulent mixing of flow, subsequently enhancing the heat dissipation performance and protecting the reliability and life of devices. Given their inexpensive and simple structure, pin-fins have extensive applications. Applications of pin-fins in the cooling configuration of a channel with cross-flow include the internal cooling of turbine blades, the cooling of electronic components and various other heat exchange devices. Short pin-fins or long pin-fins are used to suit the application. Short pin-fins typically refer to a relative fin height (H/d, where H is the fin height and d is the fin diameter) of under four, while long pin-fins have an H/d ratio of over four. The relative fin height (H/d) affects the heat transfer of pin-fins, and other affecting factors include the velocity of fluid flow, the thermal properties of the fluid and the pin-fins, the cross-sectional shape of the pin-fins, the relative inter-fin pitch, the arrangement of the pin-fins and the shroud clearance (bypass effect), among others. Many researchers have considered the effects of the aforementioned parameters on heat transfer of pin-fins. Some are summarized below.

1.1. Circular pin-fins

Vanfossen [1] and Brigham and Vanfossen [2] studied the heat transfer by short pin-fins in staggered arrangements. According to their results, longer pin-fins ($H/d = 4$) transfer more heat than shorter pin-fins ($H/d = 1/2$ and 2) and the array-averaged heat transfer with eight rows of pin-fins slightly exceeds that with only four rows. Their results also established that the average heat transfer coefficient on the pin surface is around 35% larger than that on the endwalls. Metzger et al. [3] investigated the effects of pin-fin shape and array orientation on the heat transfer and the pressure loss in pin-fin arrays. According to their

* Corresponding author. Tel.: +886 7 6256040; fax: +886 4 7357193.
E-mail addresses: tm.jeng@msa.hinet.net, t_m_jeng@yahoo.com.tw (T.-M. Jeng).

0017-9310/$ - see front matter © 2006 Elsevier Ltd. All rights reserved.
doi:10.1016/j.ijheatmasstransfer.2006.10.028

Nomenclature

a_{fs}	heat transfer surface area per unit bulk volume (m^2/m^3)
A	cross-sectional area of the test channel (m^2)
A_{base}	bottom area of the test channel, $L \times W$ (m^2)
A_{front}	frontal area of the pin-fins (m^2)
A_{total}	total heat dissipation area of pin-fins (m^2)
C_p	specific heat capacity (J/kg °C)
d	thickness or diameter of pin-fins (m)
f_d	friction factor, $f_d = \frac{\Delta P}{0.5\rho u^2}\frac{d}{L}$
h_{fs}	interstitial heat transfer coefficients between fluid stream and solid matrix (W/m^2 °C)
H	height of the channel or pin-fins (m)
k	conductivity (W/m °C)
L	length of the channel (m)
Nu_d	fin Nusselt number, $Nu_d = \frac{h_{fs}d}{k_f}$
Nu_d^*	global Nusselt number, $Nu_d^* = Nu_d \frac{A_{total}}{A_{base}}$
Pr	Prandtl number, $Pr = \frac{\mu/\rho_f}{k_f/(\rho C_p)_f}$
Re	Reynolds number based on L, $Re = \frac{\rho_f UL}{\mu}$
Re_d	Reynolds number based on d, $Re_d = \frac{\rho_f Ud}{\mu}$
S_L	center-to-center longitudinal distance between the adjacent fins (m)
S_T	center-to-center transverse distance between the adjacent fins (m)
T	volumetric average temperature (°C)
T_{final}	final temperature of preheating air at the channel inlet (°C)
U	volumetric average fluid velocity (m/s)
U_{max}	maximum velocity between fins, $U\frac{A}{A-A_{front}}$ (m/s)
W	width of the heat sink (m)
x	streamwise Cartesian coordinate (m)
X	nondimensional Cartesian coordinate, $X = \frac{x}{L}$
X_L	relative longitudinal pitch, S_L/d
X_T	relative transverse pitch, S_T/d
ΔP	pressure drop (Pa)

Greek symbols

ε	porosity of pin-fin array
μ	viscosity of fluid (kg/m/s)
ρ	density (kg/m^3)
θ	nondimensional temperature, $\theta = \frac{T-T_0}{T_{final}-T_0}$
τ	nondimensional time, $\tau = \frac{t}{L/U}$

Subscripts

0	initial
f	fluid stream
in	at channel inlet
out	at channel outlet
s	solid matrix

results, the use of circular pin-fins with an array orientation between staggered and in-line can sometimes promote the heat transfer, while substantially reducing pressure. When oblong pin-fins are used, heat transfer increases of around 20% over the circular pin-fins were measured, but these increases were offset by increases in the pressure loss of around 100%. Their estimate indicated that the pin-fin surface coefficients were approximately double the endwall values.

Numerous works [4–9] have been conducted on long pin-fins. Zukauskas and Ulinskas [4] presented famous correlations between heat transfer and pressure drop for in-line and staggered banks of tubes over wide ranges of Reynolds numbers and relative transverse and longitudinal pitches. Armstrong and Winstanley [5] reviewed how pin-fin height and inter-fin pitch affect heat transfer and flow friction, as well as the effect of accelerating flow in converging pin-fin channels. Jubran et al. [6] found that the optimal inter-fin pitch in both transverse and longitudinal directions was 2.5 times the diameter of the pin-fin, independently of both the arrangement of the pin-fins and the shroud clearance. Tahat et al. [7,8] revealed that, for in-line and staggered arrays, the ratios of the optimal transverse and longitudinal pitches to the pin-fin diameter required to maximize the heat transfer from the pin-fin assembly, were 1.3 and 2.2, respectively. Babus'Haq et al. [9] reported that the optimal ratio of the inter-fin pitch to the pin-fin diameter in the transverse direction was 2.04 for all pin-fin systems. However, the optimal ratios in the longitudinal direction were 1.63, 1.71 and 1.95 for polytetrafluoroethene pin-fins ($k = 1.7$ W/m °C), mild-steel pin-fins ($k = 54$ W/m °C) and duralumin pin-fins ($k = 168$ W/m °C), respectively. Notably, the optimal inter-fin pitches [6–9] are determined by the assembly of the channel and the base of the pin-fin array. Restated, for the test cases with small ratios of the transverse pitch to the pin-fin diameter, the distance from the base of the pin-fin array to the sidewall of the channel significantly exceeds the inter-fin space [6–9].

1.2. Square pin-fins

Grannis and Sparrow [10] used the typical experiments to verify the accuracy of the numerical simulation of fluid flow through a diamond-shaped pin-fin array. They provided the correlation between the friction factor and the Reynolds number based on the results of numerical calculations. You and Chang [11,12] adopted experimental data to elucidate numerically the fluid flow and heat transfer characteristics of square pin-fin arrays that are fully confined in a rectangular channel. By applying the porous approach. Kim and Kuznetsov [13], and Kim et al. [14] modeled pin-fin heat sinks as porous media and examined their fluid flow and heat transfer performance in a jet impinging channel and a cross-flow channel, respectively. Saha and Acharya [15] numerically studied flow and heat transfer in a periodic array of cubic pin-fins housed inside

a channel. The pin-fins are arranged in an in-line pattern with both streamwise and transverse periodicity set to 2.5 times the pin-fin dimension. Three dimensional computations and unsteady k–ε turbulence model were employed in their work. Most of them focused on the pin-fin array with the in-line arrangement and uniform distribution (meaning that the transverse pitch equalled the longitudinal pitch); they did not consider an array with non-uniform distribution. Sara et al. [16] also studied the drop in pressure and the transfer of heat in rectangular channels with square pin-fins in in-line arrangements. They considered fixed transverse pitch but variable longitudinal pitch. Square pin-fins in staggered arrangements have seldom been investigated, and only Sara [17] investigated heat transfer on large relative pitches.

Following the cited literature, this work explores the pressure drop and the heat transfer in square pin-fins with small and independently variable inter-fin pitches, to improve our understanding of pin-fin arrays. A series of experiments are systematically performed to elucidate the effects of the inter-fin pitch and the arrangement (in-line and staggered types). The performance of square pin-fins as cooling devices is compared with that of circular pin-fins. Empirical formulas for the pressure loss and the heat transfer are suggested. Accordingly, the results can help cooling engineers design more efficient cooling devices based on pin-fin arrays.

2. Experimental apparatus

Fig. 1 presents an experimental setup for measuring the flow drag and the heat transfer of pin-fin arrays. It comprises three main parts: (1) the wind tunnel, (2) the test section and (3) the data acquisition equipment. The details of the apparatus follow.

(1) *Wind tunnel*: An open-looped suction-type wind tunnel was used herein. Firstly, a one-HP blower drove air into the wind tunnel through a $200 \times 200\ \text{mm}^2$ bell mouth with a honeycomb straightener. Then, the air passed through a contraction section to reduce the turbulence. Finally, the air entered the test section after it flowed through a specially designed plate heater made of stainless steel foil. An inverter was employed to control the rate of rotation of the blower's motor to yield a specific flow rate.

(2) *Test section*: The test section was a rectangular channel that contained a square pin-fin array. The channel section was 81.5 mm wide, 76.5 mm high and 300 mm long. The channel walls were made of 20 mm thick Bakelite to reduce heat loss. The square pin-fin with a cross section of $9.6 \times 9.6\ \text{mm}^2$ and a height of 76.5 mm (i.e., $H/d = 8.0$) was made from aluminum alloy ($\rho = 2710\ \text{kg/m}^3$, $C_p = 1256\ \text{J/kg}\ ^\circ\text{C}$). The variable parameters of the pin-fin array were the relative transverse pitch ($X_\text{T} = S_\text{T}/d = 1.5$, 2.0, 2.8 where S_T is the transverse distance between the centers of adjacent fins and d is the thickness of the square pin-fin), the relative longitudinal pitch ($X_\text{L} = S_\text{L}/d = 1.5$, 2.0, 2.8 where S_L is the longitudinal distance between the centers of adjacent fins) and the arrangement of the pin-fins (in-line or staggered) (Fig. 2).

(3) *Data acquisition equipment*: The Pitot tube and the micro-manometer measured the air velocity across the test channel. The digital pressure transmitter measured pressure drops across the pin-fin arrays. The time histories of the inlet and outlet air temperatures

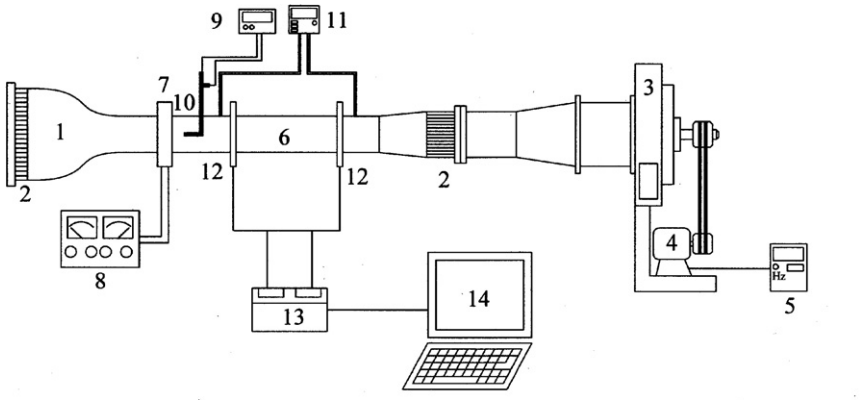

1. wind tunnel
2. honey-comb
3. blower
4. motor
5. Inverter
6. test section
7. heater
8. power supply
9. micro-manometer
10. pitot tube
11. pressure transmitter
12. thermocouples
13. recorder
14. computer

Fig. 1. Experimental setup.

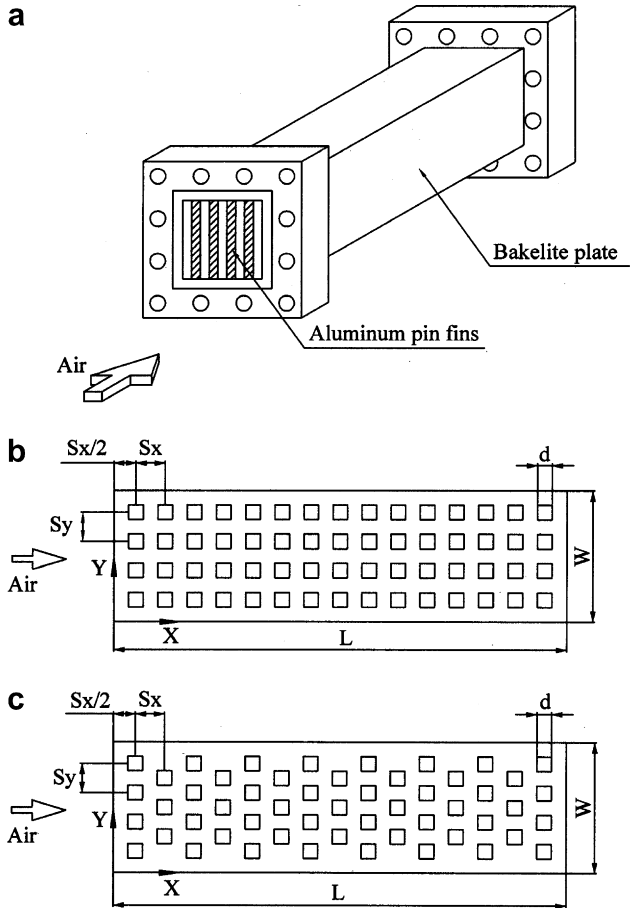

Fig. 2. Test section: (a) test section, (b) top view (in-line), and (c) top view (staggered).

were obtained using T-type thermocouples. Eighteen thermocouples were installed at the cross-sections of the channel inlet and outlet. The transient temperature signals were transferred and subsequently recorded using a real-time hybrid recorder (Agilent 34970A) at a sample rate of 2 Hz.

3. Analysis

In the transient single-blow experiments herein, a heated fluid flow supplies thermal energy to aluminum pin-fins. The fluid temperatures and the volumetric average fluid velocity in the test channel are assumed to be uniform. The temperatures of the solid and the fluid in the test channel depended on the distance along the flow direction and on the time. Therefore, this problem can be solved using a one-dimensional transient heat transfer model. The other assumptions and simplifications are as follows: (1) the pin-fin array is treated as a porous medium; (2) the fluid flow is in the steady-state and incompressible; (3) the thermophysical characteristics of the fluid and the porous media are constant, and (4) the conduction and dispersion in the flow direction are negligible. Accordingly, the volume-averaged conservation equations of energy for the solid and fluid phases are [18].

$$(1-\varepsilon)(\rho C_p)_s \frac{\partial T_s}{\partial t} = h_{fs} a_{fs}(T_f - T_s) \tag{1}$$

$$(\rho C_p)_f \left(\varepsilon \frac{\partial T_f}{\partial t} + U \frac{\partial T_f}{\partial x}\right) = h_{fs} a_{fs}(T_s - T_f) \tag{2}$$

In these equations, ε denotes the porosity of the pin-fin array, i.e., the total void volume divided by the total volume occupied by the pin-fins and void volume; U is the volumetric average fluid velocity; T_s and T_f represent the volumetric average temperature of the solid and fluid phases, respectively; h_{fs} is the interstitial heat transfer coefficient between the fluid stream and the solid matrix, and a_{fs} is the surface area of heat transfer per unit bulk volume in the test channel. Introducing the variables,

$$X = \frac{x}{L}, \quad \tau = \frac{t}{L/U}, \quad \theta = \frac{T - T_0}{T_{final} - T_0}, \quad C_1 = \frac{(\rho C_p)_f}{(\rho C_p)_s},$$
$$Pr = \frac{\mu/\rho_f}{k_f/(\rho C_p)_f}, \quad Re = \frac{\rho_f U L}{\mu}, \quad Nu_{fs} = \frac{h_{fs} a_{fs} L^2}{k_f} \tag{3}$$

enables the governing equations to be nondimensionalized as

$$(1-\varepsilon)\frac{\partial \theta_s}{\partial \tau} = C_1 \frac{Nu_{fs}}{RePr}(\theta_f - \theta_s) \tag{4}$$

$$\varepsilon \frac{\partial \theta_f}{\partial \tau} + \frac{\partial \theta_f}{\partial X} = \frac{Nu_{fs}}{RePr}(\theta_s - \theta_f) \tag{5}$$

The nondimensional forms of the initial and boundary conditions are

$$\theta_s(0,x) = \theta_f(0,x) = 0 \tag{6}$$

$$\theta_f(t,0) = \text{measured data} \tag{7}$$

The control-volume-based finite-difference technique [19] is employed to solve the above equations associated with the initial and boundary conditions. The transient finite-difference form of the energy equations is obtained explicitly by line-by-line iteration. The sensitivity of the outlet air temperature to the number of nodes and the time increment is examined to investigate the stability and accuracy of the numerical scheme. Three sets of 41, 61 and 81 nodes are adopted to ensure that the results herein are independent of the grid used. Comparing θ_f at the channel outlet between the sets of 61 nodes and 81 nodes reveals a deviation of less than 1%, indicating that 61 nodes suffice to yield grid-independent results. Additionally, the effect of the time step on the results is studied using three time steps – $\Delta\tau = 0.05$, 0.1 and 0.2. The results indicate no significant difference between the results obtained using the time steps 0.05 and 0.1. Hence, all of the calculations are performed using 61 nodes and $\Delta\tau = 0.1$.

4. Determining h_{fs} and error analysis

Fig. 3 presents a flow chart for the determination of the interstitial heat transfer coefficient in the test channel by the transient single-blow method [20,21]. The transient

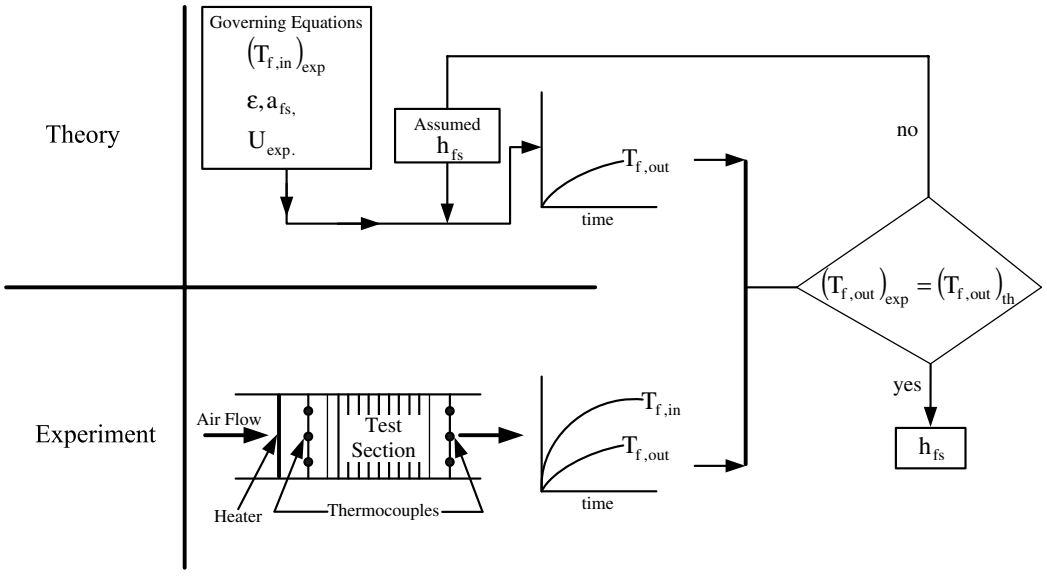

Fig. 3. Flow chart of the transient single-blow technique.

histories of the outlet air temperature ($T_{f,out}$) are governed by many parameters, including the inlet air temperature ($T_{f,in}$), the volumetric average fluid velocity (U), the porosity of the pin-fin array (ε), the heat transfer surface area per unit bulk volume (a_{fs}) and the interstitial heat transfer coefficient (h_{fs}). The test channels with various X_T, X_L and arrangements have various ε and a_{fs}. Eqs. (1)–(7) in Section 3 determine the total temperature field. The values of $T_{f,in}$, U, ε and a_{fs} can be measured. Substituting the measured data and the guessed h_{fs} into the governing equations yields the predicted outlet air temperature numerically. If the predicted outlet air temperature matches the experimental value, then the guessed h_{fs} is the interstitial heat transfer coefficient of the test channel with the specified X_T, X_L and arrangement. Fig. 4 illustrates the predicted and measured outlet air temperature of square pin-fins with in-line arrangements and various inter-fin pitches and flow rates. According to our results, the predicted outlet air temperature correlates well with the experimental value because the estimate of h_{fs} was accurate.

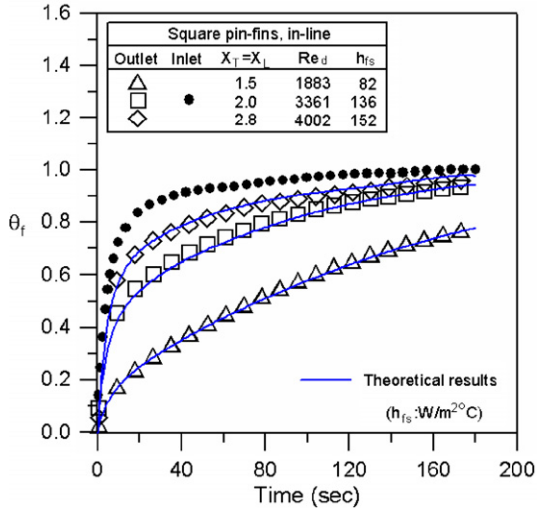

Fig. 4. The measured nondimensional inlet and outlet temperature for typical cases.

The measured volumetric average fluid velocities (U), pressure drops (ΔP) and interstitial heat transfer coefficients (h_{fs}) were used to calculate the Reynolds numbers, the friction factors and the average fin Nusselt numbers:

$$Re_d = \frac{\rho_f U d}{\mu} \tag{8}$$

$$f_d = \frac{\Delta P}{0.5\rho_f U^2}\frac{d}{L} \tag{9}$$

$$Nu_d = \frac{h_{fs} d}{k_f} \tag{10}$$

where d and L are the thickness of the square pin-fin and the length of the test channel, respectively. Data supplied by the manufacturer of the instruments stated that the measurements of flow velocity, length scale and pressure drop have an error of ±1%. The uncertainty in the measured temperature was ±0.2 °C. The inlet air was typically heated from 20 to 60 °C. Each experiment took around 180 sec. In the transient single-blow experiments, the deviation in the h_{fs} value was caused by the inlet air temperature ($T_{f,in}$), the outlet air temperature ($T_{f,out}$), the volumetric average fluid velocity (U), the porosity of the pin-fin array (ε) and the heat transfer surface area per unit bulk volume (a_{fs}). In the typical case with $X_T = X_L = 2.0$ and $Re_d = 3361$, the measurement errors in $T_{f,in}$, $T_{f,out}$, U, ε and a_{fs} yielded uncertainties of ±4.2%, ±4.6%, ±3.0%, ±3.2% and ±2.2% in h_{fs}. The standard single-sample uncertainty analysis, recommended by Kline and McClintock [22] and Moffat [23], yielded uncertainties in the Reynolds number, friction factor and average fin Nusselt number of ±2.0%, ±2.4% and ±8.1%, respectively.

5. Results and discussion

5.1. Pressure drop

Flow of a fluid through a pin-fin array exerts a force on each pin-fin, the direction of which is not necessarily coincident with that of the flow. The total drag force is the sum of the skin friction and the form drag. Its longitudinal component is called the drag force. Skin friction is responsible for almost all of the drag force at low flow rate. As the flow rate increases, the contribution of the skin friction to the drag force decreases; the rest of this force is caused by form drag. The drag causes a drop in pressure across the pin-fin array. The pressure drop is generally proportional to the flow rate at low flow rates, but to the square of the flow rate at high flow rates. This work introduces a nondimensional parameter ($f_d Re_d^2$) to represent the pressure drop to study the relationship between the pressure drop and the flow rate, and to make the experimental data more useful. This section uses the nondimensional pressure drop ($f_d Re_d^2$) and the Reynolds number (Re_d) to elucidate the relationship between the pressure drop and the flow rate through the pin-fin array.

Fig. 5 plots the nondimensional pressure drop ($f_d Re_d^2$) against Reynolds number (Re_d) for circular pin-fins with in-line arrangements, to confirm the accuracy of the flow experiments. The results indicate that, over the range of Re_d studied herein, the relative longitudinal pitch (X_L) barely affects the nondimensional pressure drop ($f_d Re_d^2$), which, however increases strongly as the relative transverse pitch (X_T) declines. The $f_d Re_d^2$ is proportional to the square of Re_d, indicating that the form drag dominates the pressure drop over the Re_d range of interest ($697 \leqslant Re_d \leqslant 10{,}960$). Least square analysis of the presented experimental data shows that all of the data concerning flow experiments on circular pin-fins in in-line arrangements satisfy the following equations:

$$\begin{aligned} f_d &= 2.00 \quad \text{for } X_T = 1.5 \\ f_d &= 0.56 \quad \text{for } X_T = 2.0 \\ f_d &= 0.19 \quad \text{for } X_T = 2.8 \end{aligned} \tag{11}$$

The average deviation between the results of Eq. (11) and the experimental data was under 5%. Notably, Eq. (11) is independent of Reynolds number within the range of $697 \leqslant Re_d \leqslant 10{,}960$. It can be explained as follows. For porous media, the relationship between f_d and Re_d can be expressed as $f_d = 2 \times (1/Re_d/Da + F/Da^{0.5})$ [24], where $Da(=K/d^2)$ is Darcy number and F is the inertial coefficient. The permeability, K, and inertial coefficient, F, are the important factors in the relationship between the pressure drop and the velocity through the porous media, and values of K and F are based on the interior structures of the porous media. For the present range of Reynolds number ($697 \leqslant Re_d \leqslant 10{,}960$), the Re_d is sufficient large so the f_d is independent of Re_d (around $2 \times F/Da^{0.5}$).

Zukauskas and Ulinskas [4] experimentally investigated the fluid flow and heat transfer characteristics in circular pin-fins with various inter-fin pitches and arrangements, over wide ranges of Reynolds numbers and Prandtl numbers. Fig. 5 also plots the predictions obtained using the correlation between the friction factor and the Reynolds number, proposed by Zukauskas and Ulinskas [4]. The data herein are consistent with the predictions of Zukauskas and Ulinskas [4], revealing the validity of the tests performed herein.

Fig. 6 plots the relationship between the nondimensional pressure drop ($f_d Re_d^2$) and the Reynolds number (Re_d) for square pin-fins with in-line arrangements. The results demonstrate that the nondimensional pressure drop ($f_d Re_d^2$) decreases as the relative longitudinal pitch (X_L) declines, because the fluid flow is concentrated in lanes between the fin columns with small X_L, reducing the turbulent wakes of the upstream pin-fins. Therefore, the pressure

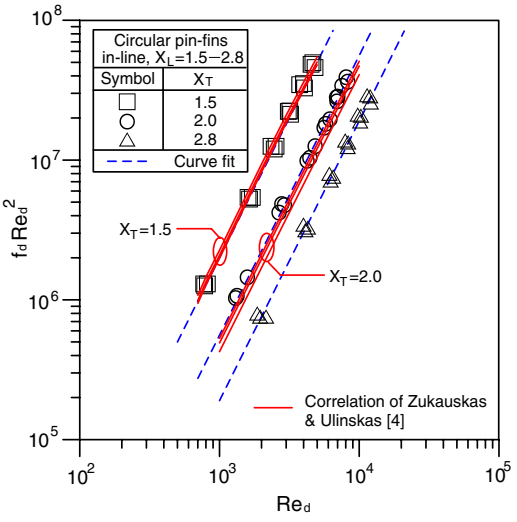

Fig. 5. Nondimensional pressure drop as a function of Reynolds number for circular pin-fins in in-line arrangements.

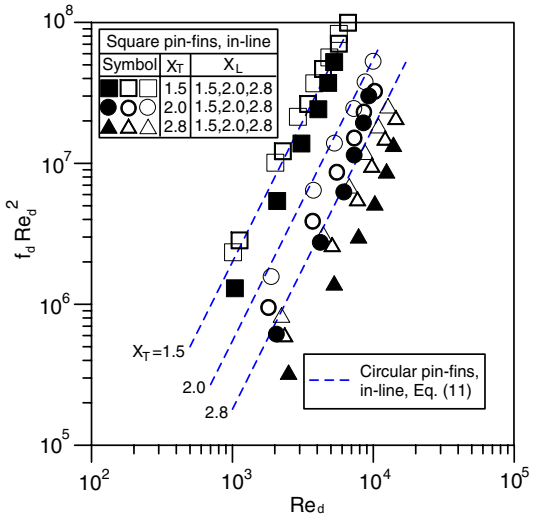

Fig. 6. Nondimensional pressure drop as a function of Reynolds number for square pin-fins in in-line arrangements.

drop falls. Moreover, as X_T decreases and Re_d increases, the effect of X_L on the pressure drop becomes weaker. However, the pressure drop falls as X_T increases. The pressure drop vs. Reynolds number studied herein can also agree with those of Jeng and Tzeng [24], who set up pin-fin arrays as porous media. They performed theoretical analysis and experimental tests to derive the correlation between the friction factor and the Reynolds number for rectangular pin-fin arrays in in-line arrangements. Fig. 6 also plots the nondimensional pressure drop for circular pin-fins in in-line arrangements, reduced using Eq. (11). The square pin-fins in in-line arrangements have smaller nondimensional pressure drops at high X_T (such as $X_T = 2.0$ or 2.8) than the circular pin-fins in in-line arrangements, but equivalent (or slightly higher) nondimensional pressure drops at low X_T (such as $X_T = 1.5$).

Fig. 7 plots the relationship between the nondimensional pressure drop ($f_d Re_d^2$) and the Reynolds number (Re_d) for square pin-fins with staggered arrangements. The results show that the nondimensional pressure drop generally falls as X_L or X_T increases. However, the effect of the inter-fin pitch on the pressure drop is weak at high Reynolds number and low X_L. The relationship between the friction factor and the Reynolds number for square pin-fins in staggered arrangements is

$$f_d = aRe_d^b \tag{12}$$

Table 1 presents the values of a and b in Eq. (12) for various inter-fin pitches, as determined by least square analysis of the presented experimental data. The average deviation between Eq. (12) and the experimental data was less than 5%. Additionally, the square pin-fins in staggered arrangements have larger nondimensional pressure drops than circular and square pin-fins in in-line arrangements.

5.2. Nusselt number

Heat is convectively dissipated by a pin-fin array by two main mechanisms – fin heat transfer and endwall heat transfer. When the relative fin height (H/d) is under 4, the pin-fin is short, and the endwall heat transfer and fin heat transfer are equally important [1–3]; when the relative fin height exceeds 4 (such as $H/d = 8$), the pin-fin is long, and the fin heat transfer is the main heat transfer path. Most researchers, in discussing the relationship between the fin heat transfer by the pin-fin array and the Reynolds number, considered the Reynolds number that is based on the maximum velocity between the pin-fins (U_{max}). U_{max} is defined as

$$U_{max} = U\frac{A}{A - A_{front}} \tag{13}$$

where A is the cross-sectional area of the test channel and A_{front} is the frontal area of the pin-fins. In order to compare the results with those of other researches, this section applies the fin Nusselt number (Nu_d) and $Re_d(U_{max}/U)$ to elucidate the relationship between the heat transfer and the maximum velocity of pin-fin arrays with various inter-fin pitches and arrangements.

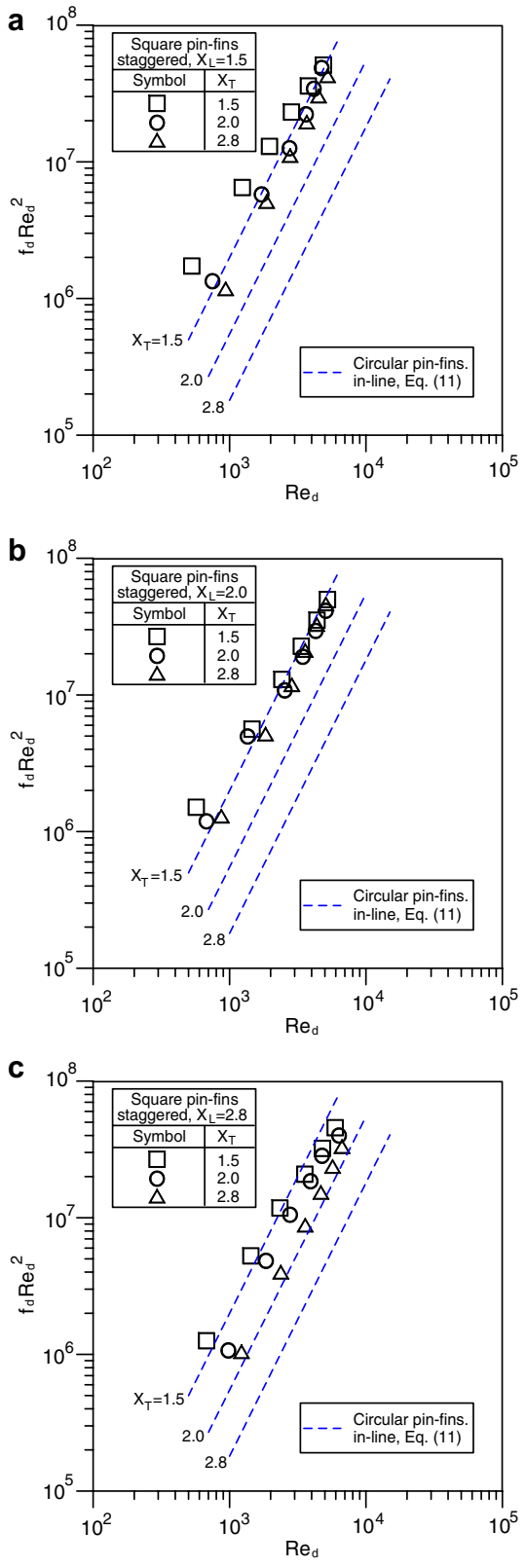

Fig. 7. Nondimensional pressure drop as a function of Reynolds number for square pin-fins in staggered arrangements: (a) $X_L = 1.5$, (b) $X_L = 2.0$, and (c) $X_L = 2.8$.

Table 1
Corresponding factors in the correlation of friction factor for square pin-fins in staggered arrangements

$f_d = aRe_d^b$ for $478 \leqslant Re_d \leqslant 6044$			
X_T	X_L	a	b
1.5	1.5	120.78	−0.472
1.5	2	2.00	0
1.5	2.8	1.46	0
2	1.5	62.69	−0.432
2	2	2.10	0
2	2.8	1.64	0
2.8	1.5	34.93	−0.374
2.8	2	1.201	0
2.8	2.8	0.701	0

Fig. 8 compares the present Nu_d values with those presented elsewhere [4–7,12,14,16,17,25]. The results indicate that the present data are within a reasonable range; in particular, the Nu_d of the circular pin-fins is very consistent with the empirical equation proposed by Zukauskas and Ulinskas [4]:

$$Nu_d = 0.237\left(Re_d \frac{U_{max}}{U}\right)^{0.63} \quad (14)$$

This work uses Eq. (14) as the basis for comparison in the follow-up. Additionally, studies of square pin-fins in in-line arrangements, such as those of You and Chang [12] and Kim et al. [14], have focused on the heat transfer of pin-fin arrays with $X_T = X_L$, Sara et al. [16] adopted fixed X_T but variable X_L. Furthermore, few studies have employed square pin-fins in staggered arrangements, and only Sara [17] investigated heat transfer for large relative pitches ($X_T = 3.25$, $X_L = 2.58$–10.33). Accordingly, this work utilizes small and independently variable inter-fin pitches ($X_T = 1.5$–2.8, $X_L = 1.5$–2.8) to study heat transfer on pin-fin arrays more thoroughly.

Fig. 9 plots the Nusselt number against Reynolds number for square pin-fins in in-line arrangements. Increasing the X_L increases Nu_d, because when square pin-fins are in in-line arrangements, if X_L is large, the airflow is not confined between the fin columns, and the effective contact area of airflow and pin-fins is increased, facilitating the heat transfer between the airflow and the pin-fins; however, the pressure drop would increases simultaneously (Fig. 6). A large X_T corresponds to a small Nu_d, because the maximum velocity between fins decreases as X_T increases. All experimental data were substituted into the empirical equation, as shown in Table 2. The average error between the values predicted using the empirical equation in Table 2 and experimental values is under 5%. Notably, Table 2 also gives the empirical equation for in-line square pin-fins with uniform distribution (for which the transverse pitch equals the longitudinal pitch), as suggested by Kim et al. [14]. When $X_T \neq X_L$ and $X_T = 2.0$, the empirical equation of Kim et al. [12] can be used to predict Nu_d accurately. However, when $X_T \neq X_L$ and $X_T = 1.5$ or 2.8, the empirical equation proposed by Kim et al. [14] deviates markedly from the present empirical equation. Fig. 9 also shows data on the Nusselt number for circular pin-fins in in-line

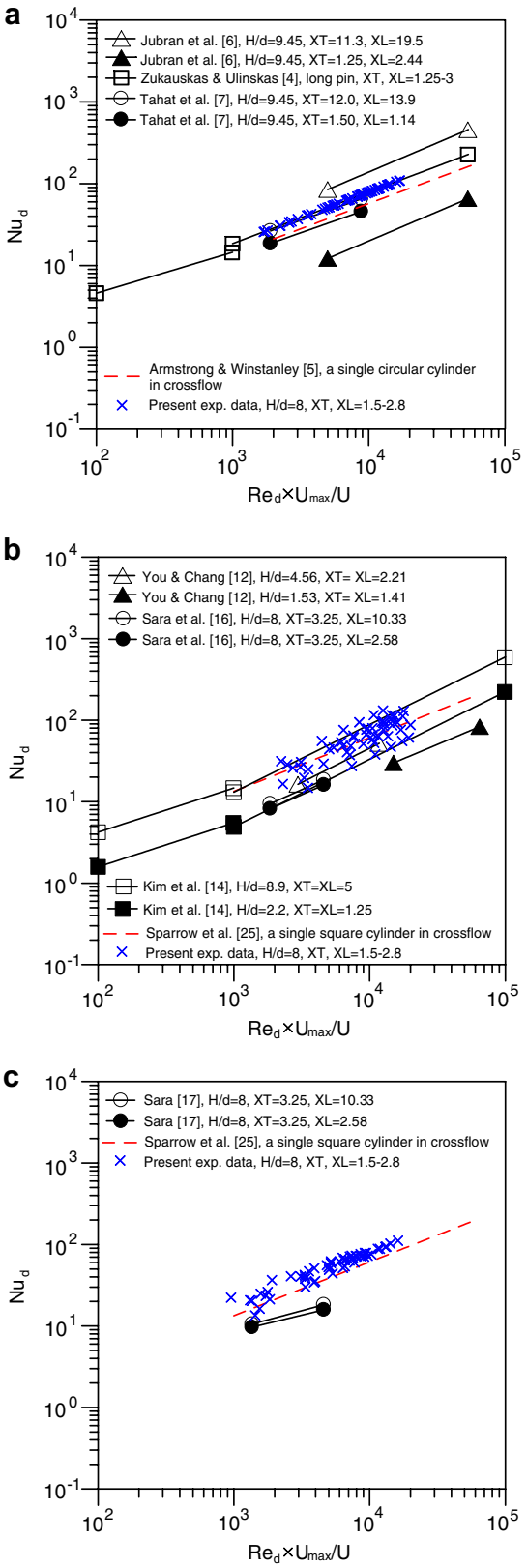

Fig. 8. Comparison of Nusselt number with others' data: (a) circular pin-fins (in-line), (b) square pin-fins (in-line), and (c) square pin-fins (staggered).

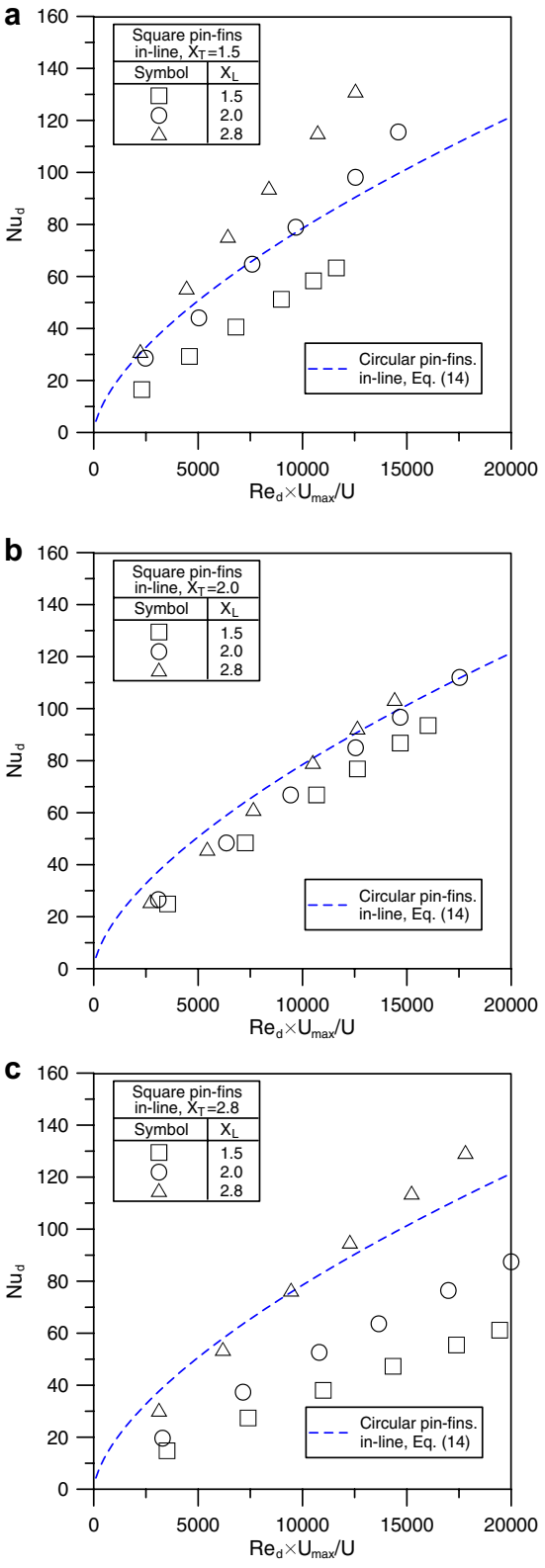

Fig. 9. Nusselt number as a function of Reynolds number for square pin-fins in in-line arrangements: (a) $X_T = 1.5$, (b) $X_T = 2.0$, and (c) $X_T = 2.8$.

arrangements (given by Eq. (14)). Most square pin-fins in in-line arrangements exhibit poorer heat transfer than circular pin-fins in in-line arrangements, but a few, such with

Table 2
Corresponding factors in the correlation of Nusselt number for square pin-fins in in-line arrangements

$Nu_d = m_1(Re_d \times U_{max}/U)^{n_1}$ for $916 \leqslant Re_d \leqslant 13{,}091$						
X_T	X_L	ε	Present work		Kim et al. [12]	
			m_1	n_1	m_1	n_1
1.5	1.5	0.607	0.0269	0.829	0.0269	0.82934
1.5	2	0.706	**0.0403**	0.829	**0.0313**	0.82934
1.5	2.8	0.79	**0.0532**	0.829	**0.0350**	0.82934
2	1.5	0.686	0.0305	0.829	0.0304	0.82934
2	2	0.764	0.0339	0.829	0.0339	0.82934
2	2.8	0.832	0.0371	0.829	0.0369	0.82934
2.8	1.5	0.764	**0.0170**	0.829	**0.0339**	0.82934
2.8	2	0.823	**0.0238**	0.829	**0.0365**	0.82934
2.8	2.8	0.874	0.0388	0.829	0.0387	0.82934

$X_L = 2.8$, show excellent heat transfer at high Reynolds number. When $X_L = 2.8$, $X_T = 1.5$ and $Re_d(U_{max}/U) = 12{,}500$, the Nusselt number ($Nu_d$) of square pin-fins is around 40% higher than that of circular pin-fins.

Fig. 10 and Table 3 shows the relationship between Nu_d and $Re_d(U_{max}/U)$ for square pin-fins in staggered arrangements. Over the range of Reynolds numbers of interest in this work, X_T and X_L negligibly affect heat transfer. When $Re_d(U_{max}/U)$ exceeds 6000, square pin-fins with staggered

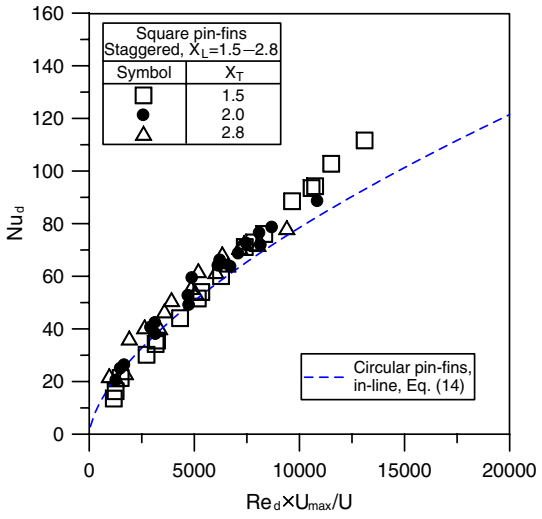

Fig. 10. Nusselt number as a function of Reynolds number for square pin-fins in staggered arrangements.

Table 3
Corresponding factors in the correlation of Nusselt number for square pin-fins in staggered arrangements

$Nu_d = m_2(Re_d \times U_{max}/U)^{n_2}$ for $478 \leqslant Re_d \leqslant 6044$ and $X_L = 1.5$–2.8		
X_T	m_2	n_2
1.5	0.058	0.796
2	0.188	0.666
2.8	0.202	0.660

arrangements generally have a high Nusselt number. When $X_T = 1.5$, $X_L = 2.8$ and $Re_d(U_{max}/U) = 12{,}500$, the heat transfer of square pin-fins in staggered arrangements exceeds that of circular pin-fins by around 20%.

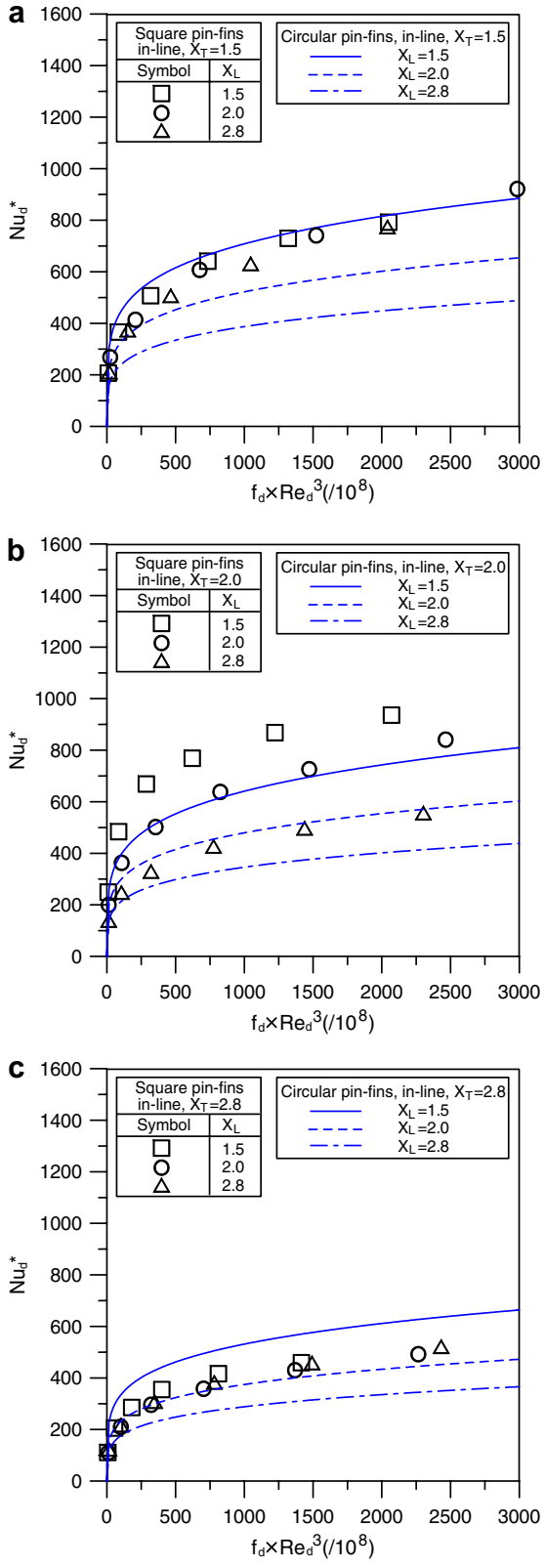

Fig. 11. Global Nusselt number as a function of nondimensional pumping power for square pin-fins in in-line arrangements: (a) $X_T = 1.5$, (b) $X_T = 2.0$, and (c) $X_T = 2.8$.

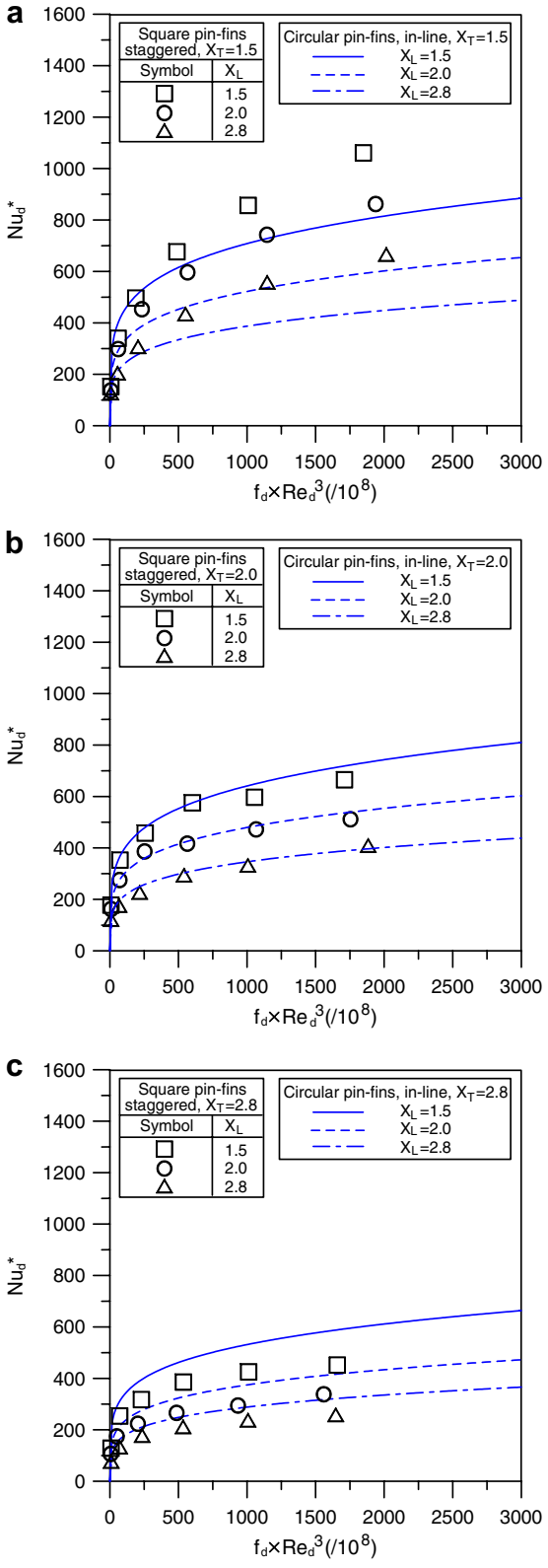

Fig. 12. Global Nusselt number as a function of nondimensional pumping power for square pin-fins in staggered arrangements: (a) $X_T = 1.5$, (b) $X_T = 2.0$, and (c) $X_T = 2.8$.

5.3. Overall performance of fluid flow and heat transfer

The convective heat dissipation of the pin-fin array in the channel is positively related to the amount of airflow that flow through it, but at high airflow, more pumping power is required to overcome the flow resistance. Therefore, in determining the optimal inter-fin pitches, the largest Nusselt number is reasonably used for a given pumping power. This section introduces $f_d Re_d^3$ as the nondimensional pumping power. Also, the fin Nusselt number (Nu_d) represents the average heat transfer capacity of the pin-fin surface, and the total heat dissipation area must be considered in determining the global heat transfer of the pin-fin array. Hence, this work proposes that Nu_d^* be used to represent the global Nusselt number, and the relationship between Nu_d^* and Nu_d is

$$Nu_d^* = Nu_d \frac{A_{total}}{A_{base}} \tag{15}$$

where A_{total} is the total area of heat dissipation of pin-fins, and A_{base} represents the bottom area of the test channel ($L \times W$).

Figs. 11 and 12 plot the global Nusselt number as function of the nondimensional pumping power for square pin-fins in in-line arrangements and staggered arrangements, respectively. The inter-fin pitches of square pin-fins in in-line arrangements are optimal at $X_T = 2$ and $X_L = 1.5$. Given a particular pumping power, the Nu_d^* is around 20% higher than that of the circular pin-fins in in-line arrangements at $X_T = 2$ and $X_L = 1.5$. For square pin-fins in staggered arrangements, the inter-fin pitches are optimal at $X_T = 1.5$ and $X_L = 1.5$, which result agrees with the optimal inter-fin pitches of circular pin-fins in in-line arrangements. Additionally, at $X_T = 1.5$ and $X_L = 1.5$ and when $f_d Re_d{}^3$ exceeds 2.5×10^{10}, the Nu_d^* of square pin-fins in staggered arrangements exceeds that of circular pin-fins in in-line arrangements; when $f_d Re_d^3 = 2.0 \times 10^{11}$, the Nu_d^* of square pin-fins in staggered arrangements is 25% higher than that of circular pin-fins in in-line arrangements.

6. Conclusions

This work experimentally investigated the pressure drop and heat transfer of a square pin-fin array in a rectangular channel using the transient single-blow technique. The variable parameters are the relative longitudinal pitch ($X_L =$ 1.5, 2, 2.8), the relative transverse pitch ($X_T = 1.5$, 2, 2.8) and the arrangement (in-line or staggered). The following conclusions are drawn:

(1) The in-line square pin-fin array has smaller pressure drop than the in-line circular pin-fin array at high X_T ($X_T = 2.0$ or 2.8) but an equivalent (or even slightly higher) pressure drop at low X_T (such as $X_T = 1.5$). Additionally, the staggered square pin-fin array has the largest pressure drop of the three pin-fin arrays (in-line circular pin-fins, in-line square pin-fins and staggered square pin-fins).

(2) Most in-line square pin-fin arrays have poorer heat transfer than an in-line circular pin-fin array, but a few, as when $X_L = 2.8$, exhibit excellent heat transfer at high Reynolds number. For instance, when $X_L = 2.8$, $X_T = 1.5$ and $Re_d(U_{max}/U) = 12{,}500$, the fin Nusselt number (Nu_d) of square pin-fins is around 40% higher than that of circular pin-fins. Moreover, when $Re_d(U_{max}/U)$ exceeds 6000, the Nusselt number of the staggered square pin-fin array generally exceeds that of the in-line circular pin-fin array. When $X_T = 1.5$, $X_L = 2.8$ and $Re_d(U_{max}/U) =$ 12,500, the heat transfer of the staggered square pin-fin array is around 20% higher than that of the in-line circular pin-fin array.

(3) The optimal inter-fin pitches are determined by the largest Nusselt number at a given pumping power. The optimal inter-fin pitches of in-line square pin-fin arrays are $X_T = 2$ and $X_L = 1.5$, its Nu_d^* is around 20% higher than that of the in-line circular pin-fin array. However, the staggered square pin-fin array performs best at $X_T = 1.5$ and $X_L = 1.5$. Furthermore, at $X_T = 1.5$ and $X_L = 1.5$ and when $f_d Re_d^3$ exceeds 2.5×10^{10}, the Nu_d^* of the staggered square pin-fin array exceeds that of the in-line circular pin-fin array; and when $f_d Re_d^3 = 2.0 \times 10^{11}$, the Nu_d^* of the staggered square pin-fin array is 25% higher than that of the in-line circular pin-fin array.

Acknowledgement

The authors would like to thank the National Science Council of the Republic of China for financially supporting this research under Contract No. NSC 95-2221-E-344-004.

References

[1] G.J. Vanfossen, Heat-transfer coefficients for staggered arrays of short pin fins, ASME J. Eng. Power 104 (1982) 268–274.
[2] B.A. Brigham, G.J. Vanfossen, Length to diameter ratio and row number effects in short pin fin heat transfer, ASME J. Eng. Gas Turbines Power 106 (1984) 241–244.
[3] D.E. Metzger, C.S. Fan, S.W. Haley, Effects of pin shape and array orientation on heat transfer and pressure loss in pin fin arrays, J. Eng. Gas Turbines Power 106 (1984) 252–257.
[4] A. Zukauskas, R. Ulinskas, Efficiency parameters for heat transfer in tube banks, Heat Transfer Eng. 6 (1985) 19–25.
[5] J. Armstrong, D. Winstanley, A review of staggered array pin fin heat transfer for turbine cooling applications, ASME J. Turbomach. 110 (1988) 94–103.
[6] B.A. Jubran, M.A. Hamdan, R.M. Abdualh, Enhanced heat transfer, missing pin, and optimization for cylindrical pin fin arrays, ASME J. Heat Transfer 115 (1993) 576–583.
[7] M.A. Tahat, R.F. Babus'Haq, S.D. Probert, Forced steady-state convections from pin-fin arrays, Appl. Energy 48 (1994) 335–351.
[8] M. Tahat, Z.H. Kodah, B.A. Jarrah, S.D. Probert, Heat transfer from pin-fin arrays experiencing forced convection, Appl. Energy 67 (2000) 419–442.
[9] R.F. Babus'Haq, K. Akintunde, S.D. Probert, Thermal performance of a pin-fin assembly, Int. J. Heat Fluid Flow 16 (1995) 50–55.

[10] V.B. Grannis, E.M. Sparrow, Numerical simulation of fluid flow through an array of diamond-shaped pin fins, Numer. Heat Transfer (Part A) 19 (1991) 381–403.
[11] H.I. You, C.H. Chang, Determination of flow properties in non-Darcian flow, ASME J. Heat Transfer 119 (1997) 190–192.
[12] H.I. You, C.H. Chang, Numerical prediction of heat transfer coefficient for a pin-fin channel flow, ASME J. Heat Transfer 119 (1997) 840–843.
[13] S.Y. Kim, A.V. Kuznetsov, Optimization of pin-fin heat sinks using anisotropic local thermal nonequilibrium porous model in a jet impinging channel, Numer. Heat Transfer (Part A) 44 (2003) 771–787.
[14] D. Kim, S.J. Kim, A. Ortega, Compact modeling of fluid flow and heat transfer in pin fin heat sinks, ASME J. Electron. Packaging 126 (2004) 342–350.
[15] A.K. Saha, S. Acharya, Unsteady simulation of turbulent flow and heat transfer in a channel with periodic array of cubic pin-fins, Numer. Heat Transfer (Part A) 46 (2004) 731–763.
[16] O.N. Sara, S. Yapici, M. Yilmaz, T. Pekdemir, Second law analysis of rectangular channels with square pin-fins, Int. Commun. Heat Mass Transfer 28 (2001) 617–630.
[17] O.N. Sara, Performance analysis of rectangular ducts with staggered square pin fins, Energy Convers. Manage. 44 (2003) 1787–1803.
[18] C.C. Wu, G.J. Hwang, Flow and heat transfer characteristics inside packed and fluidized beds, ASME J. Heat Transfer 120 (1998) 667–673.
[19] S.V. Patankar, Numerical Heat Transfer and Fluid Flow, McGraw Hill-Hemisphere, New York, 1980.
[20] C.Y. Liang, W.J. Yang, Modified single-blow technique for performance evaluation on heat transfer surfaces, ASME J. Heat Transfer 96 (1975) 16–21.
[21] J.J. Hwang, G.J. Hwang, R.H. Yeh, C.H. Chao, Measurement of interstitial convective heat transfer and frictional drag for flow across metal foams, ASME J. Heat Transfer 124 (2002) 120–129.
[22] S.J. Kline, F.A. Mcclintock, Describing uncertainties in single-sample experiments, Mech. Eng. (1953) 3–8.
[23] R.J. Moffat, Contributions to the theory of single-sample uncertainty analysis, ASME J. Fluids Eng. 104 (1986) 250–260.
[24] T.M. Jeng, S.C. Tzeng, A semi-empirical model for estimating permeability and inertial coefficient of pin-fin heat sinks, Int. J. Heat Mass Transfer 48 (2005) 3140–3150.
[25] E.M. Sparrow, J.P. Abraham, J.C.K. Tong, Archival correlations for average heat transfer coefficients for non-circular and circular cylinders and for spheres in cross-flow, Int. J. Heat Mass Transfer 47 (2004) 5285–5296.